Nucleic Acids Research, 1997, Vol. 25, No. 11 **2083–2090**

Structure of the acceptor stem of *Escherichia coli* tRNA^{Ala}: role of the G3·U70 base pair in synthetase recognition

Andres Ramos and Gabriele Varani*

MRC Laboratory of Molecular Biology, Hills Road, Cambridge CB2 2QH, UK

Received February 20, 1997; Revised and Accepted April 11, 1997

ABSTRACT

The fidelity of translation of the genetic code depends on accurate tRNA aminoacylation by cognate aminoacyl-tRNA synthetases. Thus, each tRNA has specificity not only for codon recognition, but also for amino acid identity; this aminoacylation specificity is referred to as tRNA identity. The primary determinant of the acceptor identity of *Escherichia coli* tRNA^{Ala} is a wobble G3·U70 pair within the acceptor stem. Despite extensive biochemical and genetic data, the mechanism by which the G3·U70 pair marks the acceptor end of tRNA^{Ala} for aminoacylation with alanine has not been clarified at the molecular level. The solution structure of a microhelix derived from the tRNA^{Ala} acceptor end has been determined at high precision using a very extensive set of experimental constraints (~32 per nt) obtained by heteronuclear multidimensional NMR methods. The tRNA^{Ala} acceptor end is overall similar to A-form RNA, but important differences are observed. The G3·U70 wobble pair distorts the conformation of the phosphodiester backbone and presents the functional groups of U70 in an unusual spatial location. The discriminator base A73 has extensive stacking overlap with G1 within the G1·C72 base pair at the end of the double helical stem and the -CCA end is significantly less ordered than the rest of the molecule.

INTRODUCTION

The fidelity of translation of the genetic code depends on accurate tRNA aminoacylation by aminoacyl-tRNA synthetase (aaRS) enzymes. Functional studies (1–4) have identified sets of identity elements, i.e. nucleotides specific to each tRNA, responsible for efficient discrimination between different tRNAs by aaRS enzymes. Crystallographic structures of Gln, Asp, Ser and Lys tRNAs in complex with cognate synthetases (5–12) have provided important insights into the structural basis of tRNA–synthetase recognition and discrimination. Detailed structural information is still missing for the remaining tRNA–synthetase systems.

The primary determinant of *Escherichia coli* tRNA^{Ala} identity is the G3·U70 wobble pair (Fig. 1a). Conversion of the G3·U70 pair to G·C or A·U eliminates aminoacylation with alanine *in vivo* and *in vitro* (13,14); introduction of a G·U base pair within the acceptor end of other tRNAs confers alanine identity to that tRNA (13,14). AlaRS even binds (15) and aminoacylates (16,17) microhelices derived from the acceptor stem, although with reduced efficiency compared with the full tRNA (17–19).

In addition to tRNA^{Ala}, G·U wobble pairs provide recognition signals in several ribozymes (20–22). It is remarkable how often this simple structural element has been selected to define unique recognition sites for protein and RNA enzymes. The importance of G·U wobble pairs in intermolecular recognition has motivated extensive biochemical and genetic studies to understand the molecular mechanism underlying tRNA^{Ala} identity. One possible mechanism is the direct recognition by the alanyl synthetase of unique functional groups exposed on the G3·U70 pair. In support of this proposal, *in vitro* studies with microhelix substrates demonstrated that the exocyclic amine of G3 is critical for aminoacylation with alanine (19,23). A second hypothesis (that does not exclude the first) proposes instead that the G·U base pair is recognized primarily through its unique conformational features ('indirect recognition'). In support of indirect recognition, it was found that the G3·U70 pair in tRNA^{Ala} can be substituted *in vivo* with other non-Watson–Crick base pairs without loss of alanine identity (24–26). Initial NMR investigations of a tRNA^{Ala} microhelix duplex suggested that the wobble pair introduces a helical distortion in the tRNA^{Ala} acceptor end (27) and revealed that the ACCA end thermodynamically stabilizes the acceptor end (28). In this manuscript we present the high resolution structure of the tRNA^{Ala} acceptor end microhelix. This structure illustrates how the G3·U70 base pair provides not only a unique array of functionalities in the major and minor grooves, but also distinctive structural features for intermolecular recognition.

MATERIALS AND METHODS

RNA synthesis

The 22mer tRNA^{Ala} acceptor end microhelix (Fig. 1a) was synthesized by *in vitro* transcription using T7 RNA polymerase and synthetic DNA templates and purified by standard methods using denaturing polyacrylamide gel electrophoresis (29). Aliquots of 15 ml transcription reaction yielded ~90 OD units (~5 mg) of fully purified 22mer RNA. Since the RNA was produced by *in vitro* transcription, the 5′-end of the RNA is phosphorylated. Isotopically

*To whom correspondence should be addressed. Tel: +44 1223 402 417; Fax: +44 1223 213 556; Email: gv1@mrc-lmb.cam.ac.uk

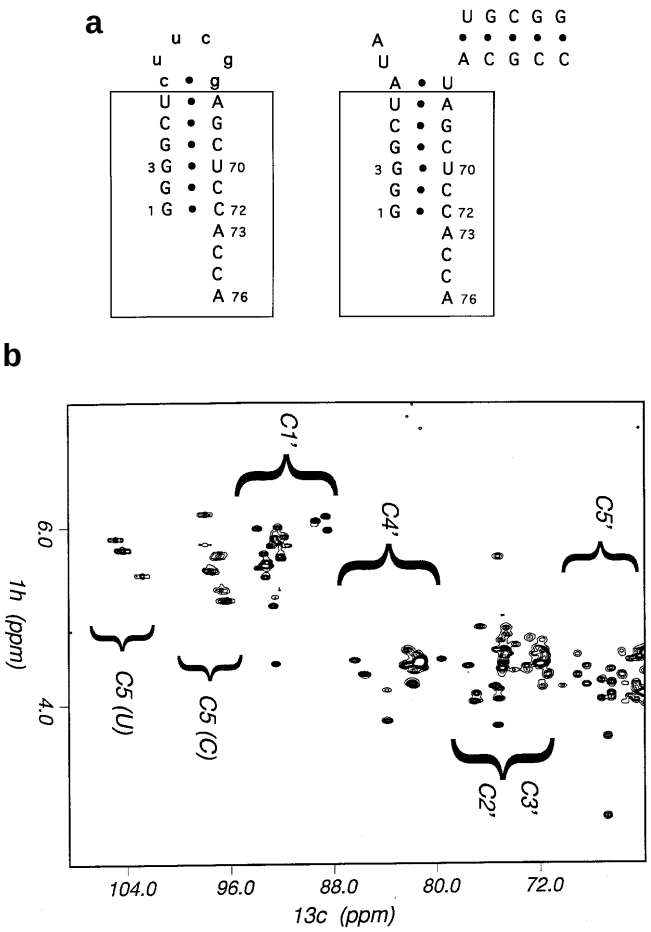

Figure 1. (**a**) Secondary structures of the acceptor end microhelix used in the present investigation (left) and the *E.coli* $tRNA^{Ala}$ acceptor stem (right). (**b**) Sugar region of the ^{1}H-^{13}C HSQC spectrum of the $tRNA^{Ala}$ microhelix.

labelled RNAs were synthesized using ^{15}N- or $^{13}C/^{15}N$-labelled ribonucleotides (30). Three NMR samples were prepared with either unlabelled, ^{15}N-labelled or ^{13}C-^{15}N labelled RNA. The final concentrations of all samples were 1.5–2 mM in 0.1 mM EDTA, 5 mM phosphate buffer, pH 5.2; no mono- or divalent cations were added.

NMR spectroscopy

NMR spectra were acquired with Bruker AMX-500 or DMX-600 spectrometers equipped with triple resonance gradient probes. Data were processed using Felix 2.30 (Biosym). Multidimensional datasets were zero-filled to an appropriate size after multiplication of the time domain data with shifted sine-bell functions. Spectral assignments were obtained from an extensive set of multidimensional heteronuclear experiments, as previously described in other publications from our laboratory (29,31–33; a table of assignments can be obtained directly from the authors). Briefly, 2- and 3-dimensional ^{15}N- and ^{13}C-edited NOESY spectra recorded in H_2O were used to assign base imino and amino resonances. Assignments of sugar resonances were obtained from 3-dimensional correlated experiments utilizing ^{13}C-^{13}C transfer. ^{31}P assignments were obtained from 2-dimensional ^{1}H-^{31}P experiments and 3-dimensional triple resonance ^{1}H-^{13}C-^{31}P experiments (29,34). A representative spectrum is shown in Figure 1b.

Constraints for structure determination

Numbers and categories of experimental constraints are shown in Table 1. Distance constraints between non-exchangeable protons were obtained from 2-dimensional NOESY build-ups (50, 100 and 150 ms mixing times) and two 3-dimensional NOESY-HMQC spectra recorded in succession at 50 and 150 ms mixing time. Cross-peaks corresponding to H5–H6 resonances in pyrimidines and to other covalently constrained distances were volume-integrated using Felix 2.30. Most NOE build-up rates were linear up to 150 ms mixing time, although H5′–H5″ cross-peaks (at a fixed 1.8 Å distance) deviated from linearity above 100 ms mixing times. This analysis provided reliable calibrations for preparation of the constraint list. Cross-peaks with volumes ≥H5–H6 peaks at 50 ms mixing time were attributed upper limits of 2.8 Å (‘strong’ peaks); cross-peaks with volumes at 150 ms mixing time ≥H5–H6 cross-peaks at 50 ms (‘medium’ peaks) were attributed 3.3 Å upper limits; ‘weak’ cross-peaks (intensity at least as large as that of H1′–H3′ peaks at 50 ms mixing time) were attributed an upper limit of 4.0 Å (the H1′–H3′ distance is between 3.6 and 3.9 Å for all sugar conformations). Cross-peaks weaker than H1′–H3′ peaks or cross-peaks that could not be volume-integrated reliably due to partial spectral overlap were attributed 5.0 Å upper limits. However, cross-peaks observed only in 3-dimensional NOESY spectra at long mixing time (150 ms) were given a generous upper limit of 7 Å to reduce any systematic error due to spin diffusion. Interproton distances derived from NOE cross-peaks involving exchangeable resonances were generally given a single upper limit of 6 Å. However, cross-peaks involving base paired guanosine NH and cytosine NH_2, adenine H2 and uracil NH resonances and imino resonances from the G·U wobble pair were attributed a 4 Å upper limit. Lower distance bounds were never introduced.

A first round of structure calculations was completed using a constraint list containing ~400 distances. A list of all possible proton pairs within a 5 Å cut-off distance was then generated from the coordinates of the converged structures. This list of interproton distances was compared with the experimental constraint list and NOESY spectra were re-examined to identify ambiguous NOE cross-peaks. This iterative procedure was repeated several times, leading to the identification of ~165 additional, mostly interresidual, distance constraints. In the end, all close contacts predicted from the structures were present in the constraint list, with the exception of distances involving overlapping sugar resonances or exchange-broadened 2′-OH, NH or NH_2 resonances.

The total number of NOE-based distance constraints was 565 (~26 per nt), including 288 interresidual constraints (~13 per nt). One hundred and thirty seven intranucleotide constraints corresponded to distances that are fixed within narrow bounds by the covalent geometry and are therefore redundant. However, it is crucial to sift through these resonances to validate spectral assignements and to identify internucleotide NOE interactions.

Hydrogen bonding constraints were introduced when a slow rate of exchange with solvent and a large downfield shift of NH and NH_2 resonances was observed, in addition to characteristic patterns of NOE interactions expected for Watson–Crick base pairs. Only constraints corresponding to the Watson–Crick base

Table 1. Statistics of experimental constraints and structural statistics for the 30 converged structures of the $tRNA^{Ala}$ microhelix

NMR structure statistics

NMR data

NOE constraints	**565**
Intraresidues	**277**
Sequential	**226**
Long Range	**62**
Average number per nucleotide:	**26**
Hydrogen bonding constraints	**38**
Dihedral constraints (α,β,γ,δ,ε,ζ)	**105**
Average number per residue	**5**
Total experimental constraints	**708**
Average number per nucleotide	**32**

Structure analysis

Average deviations from ideal covalent geometry	
Bond lenght	**0.004 Å**
Bond angles	**0.95°**
Impropers	**0.38°**
NOE violations	
Average violations in converged structures (> 0.1 Å)	**0**
Average violations in non converged structures (> 0.1 Å)	**12**
Largest violations for converged structures	**0.08 Å**
Largest violations for non converged structures	**1 Å**
Angle violation (>3°) in converged structures	**0**
r.m.s. deviations from average structure (Å)	
Full structure	**3.2 ± 1.09 Å**
Helical Stem (G1-C7; G66-C72)	**1.35 ± 0.56 Å**
Tetraloop	**0.67 ± 0.14 Å**
G1•C72 + ACCA	**2.2 ± 0.25 Å**

pairs predicted from the secondary structure were introduced at first. Hydrogen bonding constraints were introduced for the G·U base pair only after calculations conducted in their absence confirmed the wobble geometry (32). Two distance constraints were used for each hydrogen bond, one between heavy atoms (3 ± 0.3 Å) and one between the hydrogen atom and the acceptor (1.9 ± 0.1 Å).

A total of 105 dihedral angle restraints (14 α, 14 ζ, 19 β, 17 γ, 20 ε and 21 δ) obtained from semi-quantitative estimates of the magnitude of scalar coupling constants were included in the final constraint set. No *ad hoc* constraints were introduced for the glycosidic angle χ. As described (29,34), α and ζ were very loosely restrained to 0 ± 120; β, γ, δ and ε were constrained with uncertainties of ±40–60°; in some cases, partial spectral overlap led us to use even wider uncertainties. When the scalar coupling patterns indicated significant conformational averaging (e.g. for the ACCA end), dihedral angle constraints were not introduced.

Structure determination and analysis

Structure calculations by restrained molecular dynamics were performed using an X-PLOR-based (35) simulated annealing protocol (29); parameters for the sugar configuration were corrected as described (32). Dihedral energy terms designed to reproduce ideally staggered rotamers and electrostatic interactions were never included to avoid any bias from the non-covalent components of the force field. Out of 90 initial structures with random coordinates, 40 crashed during the early stages of the computations due to violations of the covalent geometry. The remaining 50 structures satisfied the experimental constraints to different extents. When energy profiles and energy-ordered r.m.s.d. profiles (29,36) of these 50 structures were analysed, the pseudo-energies of NOE violations and total energies (not shown) were very similar for the 30 best structures, but increased slightly from 31 to 40; the abrupt increase for structures 41–50 unambiguously identifies 10 structures which satisfy the experimental data very poorly or with unsatisfactory stereochemistry. Visual inspection of structures 31–40 revealed that in each case 1 bp (generally C7·G66) was not formed. Although distance constraints used to represent hydrogen bonds are nearly satisfied by a staggered conformation where the two bases are not co-planar, this conformation violates the identification of Watson–Crick base pairing. Thus, only the best 30 structures provide satisfactory agreement with the NMR data; the convergence rate (30 out of 50) is typical for RNA structures calculated in our laboratory (29). Energy-ordered r.m.s.d. profiles (29) were used to derive the r.m.s.d. figures reported in Table 1. All r.m.s.d. values reported in the text and the analysis of all conformational properties are based on the full ensemble of 30 converged structures.

Root mean square deviations to the average structure were calculated using Clusterpose (37). Statistics for dihedral angles and other conformational parameters were calculated using a program kindly provided by Dr Brian Wimberly (Scripps Research Institute). Double helical parameters were analysed using RNA (38).

RESULTS

NMR analysis and structure determination

The sequence of the 22mer RNA stem–loop used in this study (Fig. 1a) corresponds to the first 6 bp of the *E.coli* $tRNA^{Ala}$ acceptor stem; this structure was stabilized by an exceptionally stable C(UUCG)G tetraloop. Nearly complete ^{1}H, ^{13}C, ^{15}N and ^{31}P assignments were obtained using well-established methods (29). The only missing assignments are the H5′–H5″–C5′ resonances of A73 (broadened by conformational exchange) and the exocyclic amino resonances of G2, C74, C75 and A76.

Structure determination was based on the collection of hydrogen bond, dihedral angle and NOE-derived distance constraints (Table 1). Hydrogen bonding constraints are very powerful: great care is required to avoid misidentification. Strong NH–NH NOE interactions and characteristic ^{1}H and ^{15}N chemical shifts provided strong evidence for the G3·U70 base pair. However, hydrogen bonding constraints for G3·U70 were only added after structures calculated in the absence of explicit hydrogen bonding constraints consistently produced a wobble G·U pair (32). Interproton distances were divided into loose categories, avoiding the introduction of lower bounds, to reduce any systematic error from spin diffusion or other experimental artifacts. The density of internucleotide distance constraints is nearly constant throughout the structure, including the single-stranded ACCA end. Only at the tetraloop site does an unusually compact structure result in a higher density of constraints. In contrast, the density of intranucleotide constraints varies considerably, reflecting different degrees of spectral overlap for the

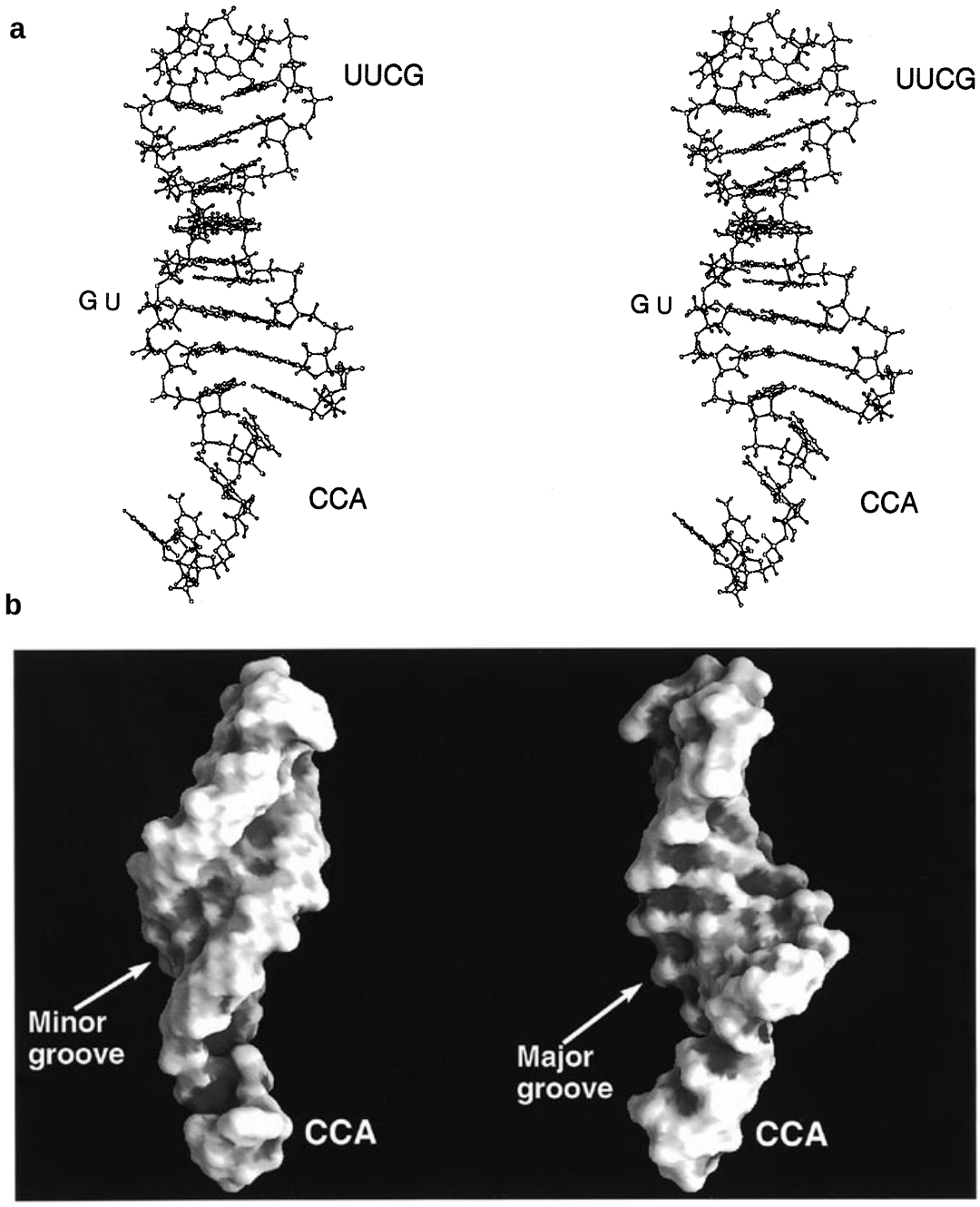

Figure 2. (**a**) Stereoview of a low energy structure of the $tRNA^{Ala}$ microhelix. (**b**) Surface representation of the structure viewed from the minor (left) and major (right) grooves.

sugar resonances. Structure calculations used an X-PLOR-based (35) restrained molecular dynamics protocol (29); electrostatics and dihedral components of the force field were turned off throughout the calculation to avoid biasing the final structure. Energy profiles and energy-ordered r.m.s.d. profiles (29) clearly separated structures with good agreement with the experimental data ('converged' structures) from structures that satisfy the experimental constraints less well ('non-converged' structures).

Structural statistics for 30 converged structures are also reported in Table 1. The UUCG tetraloop is identical to the previous structure (32) and will not be discussed further. The wobble G·U pair is slightly less precisely defined than other regions of the stem, despite an equal density of constraints. The ACCA end is much less precisely defined; averaging in the scalar coupling patterns indicates that this is due to genuine conformational flexibility.

Global structure of the $tRNA^{Ala}$ acceptor end microhelix

The overall structure of the $tRNA^{Ala}$ microhelix is close to A-form RNA (Fig. 2). This is revealed by distinctive shapes of major and minor grooves (Fig. 2b), base stacking interactions, C3′-*endo* sugar conformations and by the values of helical parameters. However, the r.m.s. deviation between an A-form

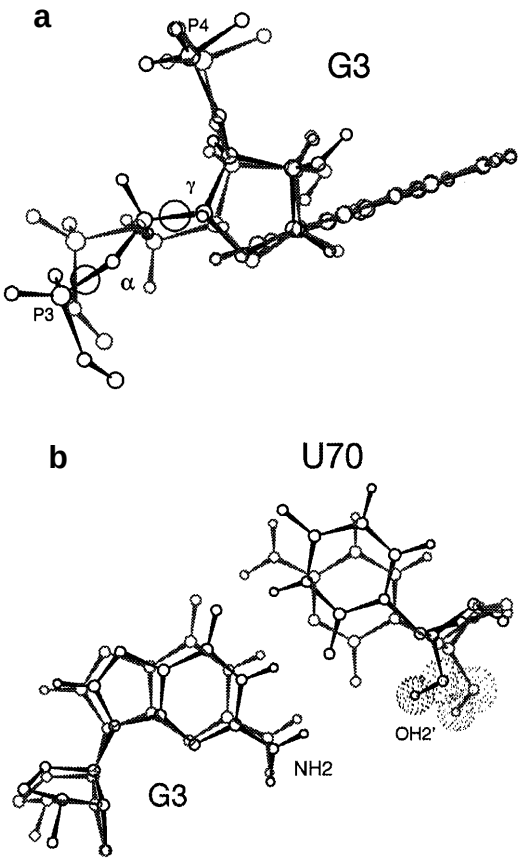

Figure 3. (**a**) The unusual values of α and γ of G3 in the tRNA^{Ala} microhelix (black) produce a distinctive conformation of the phosphodiester backbone, when compared with A-form RNA (grey). (**b**) Superimposition of the G3·U70 base pair derived from the present NMR structure (black) with a G3·C70 pair in A-form RNA (grey).

RNA stem with a G3·C70 pair and the acceptor end microhelix is 3.2 Å, revealing significant differences. A first distinction from A-form RNA is the less pronounced displacement from the helix axis (~3 Å in the present structure versus 4 Å for A-form RNA). Since extensive computer simulations indicate that the displacement should be reproduced within an accuracy of ~1 Å (39), this difference between the tRNA^{Ala} acceptor end and ideal A-form RNA is likely to be significant.

Structure of the G3·U70 wobble pair

The most significant deviations from A-form RNA are observed at the G3·U70 wobble pair. Analysis of the backbone dihedral angles reveals that the α and γ angles of G3 in the wobble pair are *trans*/*trans* instead of the common *gauche*$^-$/*gauche*$^+$ conformation (Fig. 3a). The observed pattern of scalar coupling interactions in the backbone of G3 is consistent both with conformational averaging between multiple conformers and with a static distortion from regular A-form features. Therefore, both *trans*/*trans* and *gauche*$^-$/*gauche*$^+$ ranges were allowed in the constraint list, but only the *trans*/*trans* conformation was found in every calculated structure. Attempts at imposing a *gauche*$^-$/*gauche*$^+$ conformation produced structures with significantly higher values of the energy terms corresponding to the RNA stereochemistry and to the pseudo-energy of NOE violations. The *trans*/*trans* backbone conformation has been observed for a G·U base pair in the tRNA^{Asp} crystal structure (40), in NMR (41) and crystallographic structures of U·U base pairs (42) and in a duplex containing G·A base pairs (43). The 'crankshaft' motion of the backbone changes the phosphate–phosphate distance on the purine-rich strand around the G·U pair, resulting in a ~0.8 Å displacement of the phosphate from the position expected for an ideal A-form helix. As a consequence of this backbone conformation, the G3 and G4 phosphates are more distant from each other than other phosphate pairs, whereas the following phosphates (G4 and G5) are closer.

Formation of the G·U base pair also presents the U70 nucleotide in a distinctive spatial location (Fig. 3b), but in other respects, the conformation of the G3·U70 pair is similar to that expected for a G3·C70 pair in a regular A-form helix. For example, the minor groove width (11–11.5 Å) is typical for A-form RNA (11.3 Å) and base stacking is similar to what would be expected for a G·C containing helix (Fig.4a). In contrast to the G·U pair in the P1 helix (32), but as observed crystallographically in tRNA^{Phe} (44), interstrand stacking is very limited.

Structure and dynamics of the ACCA end

In contrast to what is generally observed in blunt-ended double helices, the last base pair of the acceptor stem (G1·C72) is well defined in the present structure and the G1 imino proton is protected from exchange with solvent. Thus, the presence of the ACCA end stabilizes the G1·C72 pair, as suggested by both biochemical and NMR studies (27,28). As revealed by unusual NOE interactions, A73 overlaps predominantly with G1 rather than C72 (Fig. 4b).

Clear NOE interactions confirm that A73, C74 and C75 stack on each other in a manner not unlike that seen within each strand of a double helix. This result confirms previous, more qualitative studies of tRNA^{fMet} (45) and tRNA^{Ala} (27,28) acceptor end microhelices. However, several NMR observables and the superimposition of converged structures (Fig. 5a) reveal that the -CCA end in the present structure is considerably less ordered than in the crystal structure of tRNA^{Phe} (44) or suggested in previous NMR studies (27,45). Conformational flexibility around A73 is confirmed by averaging in scalar coupling patterns and by the selective broadening of some resonances (C5′, H5′ and H5″ of A73).

DISCUSSION

Alanyl-tRNA synthetase specifically aminoacylates tRNA^{Ala} because other tRNAs lack a G3·U70 base pair within the acceptor stem. The G3·U70 pair can contribute to tRNA^{Ala} identity by three mechanisms. First, the wobble pair presents a distinctive array of hydrogen bond donors and acceptors in the major and minor grooves. Second, unusual structural features induced by the G3·U70 pair may influence AlaRS binding to the acceptor stem and/or position the -CCA end of tRNA^{Ala} in the enzyme active site for catalysis. Third, the G3·U70 pair may destabilize the acceptor end and favour formation of an optimal active site geometry by induced fit. These mechanisms are not mutually exclusive.

The role of the functional groups in the minor groove of the acceptor stem on recognition and aminoacylation by AlaRS has been extensively investigated by *in vitro* biochemical experiments

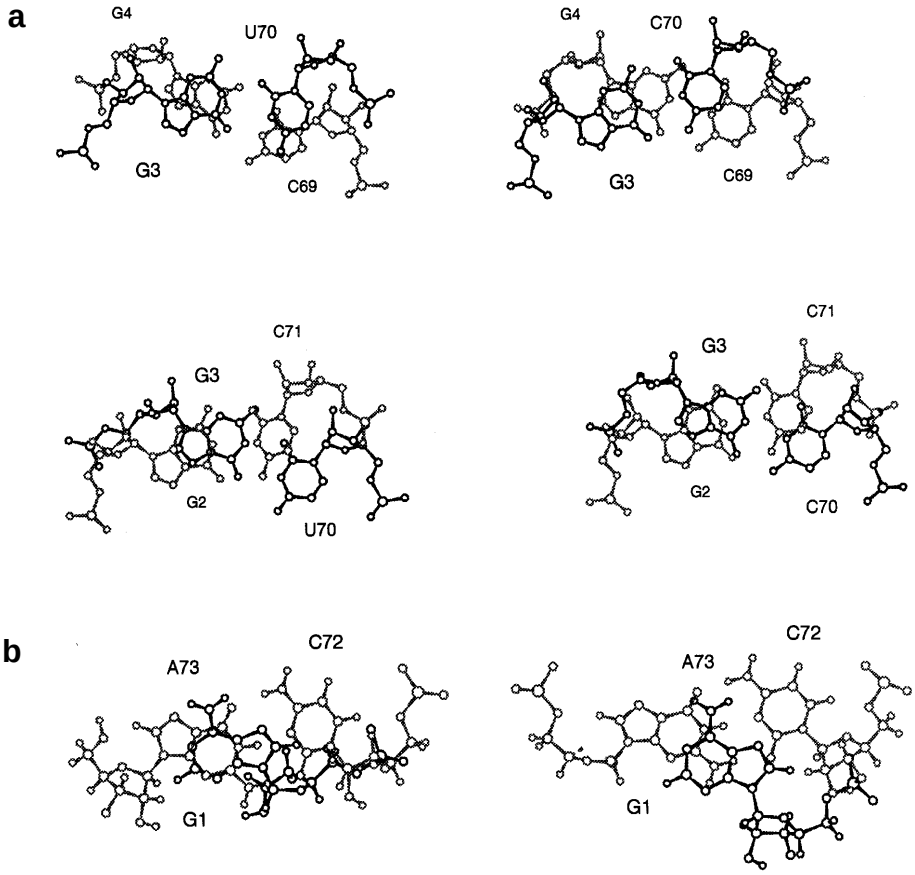

Figure 4. (**a**) Base stacking interactions at the 3·70 site in a low energy structure of the tRNA^{Ala} microhelix (left) and in A-form RNA with a G3·C70 base pair (right). The 3·70 pair is in black in all panels; the G2·C71 base pair (grey) is in the bottom panels and the G4·C69 base pair (grey) in the two top panels. (**b**) Base stacking interactions involving G1·C72 (grey) and A73 (black) in a low energy structure of the tRNA^{Ala} microhelix (left) and in A-form RNA (right).

on microhelix RNA substrates (19,23,46). The unpaired amine of G3 contributes the most to aminoacylation of microhelix substrates *in vitro*, but the amine of G2 and three 2′-OH groups (Fig. 5b) are also important. In order to investigate how the structure of the G·U pair in the acceptor end contributes to tRNA^{Ala} identity, we have examined the solution structure of the tRNA^{Ala} acceptor stem microhelix; similar model substrates bind AlaRS with $K_d \approx 10$ μM (15) and are aminoacylated with alanine *in vitro* (17). More qualitative NMR studies by Limmer and co-workers (27) did not lead to a formal structure, but the interpretation of the experimental results was generally in agreement with the present structure.

Overall, the structure of the tRNA^{Ala} acceptor stem is similar to A-form RNA, but significant deviations are observed at and around the G3·U70 wobble pair. In order to assess the significance of such deviations, the present structure was compared with other structures of helices containing G·U pairs: the NMR structure of the P1 helix from group I self-splicing introns (32) and the crystal structures of tRNA^{Phe} (44) and tRNA^{Asp} (40). This comparison reveals that the conformation of the G·U base pair within the tRNA^{Ala} microhelix is close to that of the tRNA^{Phe} acceptor end, but it is distinct from both the P1 helix and tRNA^{Asp} structures. A characteristic pattern of undertwist–overtwist was observed for the P1 helix (32) and for the U5·G68 base pair within the acceptor stem of tRNA^{Asp} (40), but not in the tRNA^{Ala} microhelix or in tRNA^{Phe}: variations in helical twist across the base pair are small (Table 2). The large and positive inclinations observed here are also similar to tRNA^{Phe} and distinct from the P1 helix. When backbone angles are examined, α and ζ are in the canonical *gauche*$^-$/*gauche*$^+$ conformation in all such structures except the tRNA^{Ala} microhelix, where they are instead *trans*/*trans*. Thus, both backbone conformers can accommodate different base stacking arrangements. The G·U base pairs are in similar sequence contexts in both the tRNA^{Ala} and tRNA^{Phe} acceptor ends, with purine nucleotides on either side of the guanosine. In the P1 helix and in tRNA^{Asp}, the wobble guanosine is instead surrounded by pyrimidines. Our results reinforce the suggestion that sequence context is a primary determinant of double helical geometry (40).

The *trans*/*trans* conformation of the phosphodiester backbone of G3 leads to unusual phosphate–phosphate distances and presents the anionic oxygens towards the exterior of the structure (Fig. 3a). This backbone structure could facilitate sequence-dependent recognition of the G3·U70 pair by an indirect mechanism (40). In addition, the wobble pair presents the 2′-OH and base functionalities of U70 in both the major and minor groove in a distinctive spatial location (Fig. 3b). The hydroxyl group of U70 makes a large contribution to tRNA^{Ala}–AlaRS discrimination (46); the role of major groove functionalities has not been experimentally tested. The distinctive base functionalities and metal binding sites in the major groove of G·U base pairs (31,47,48) may provide an array of hydrogen bonding donors and acceptors and a distinctive

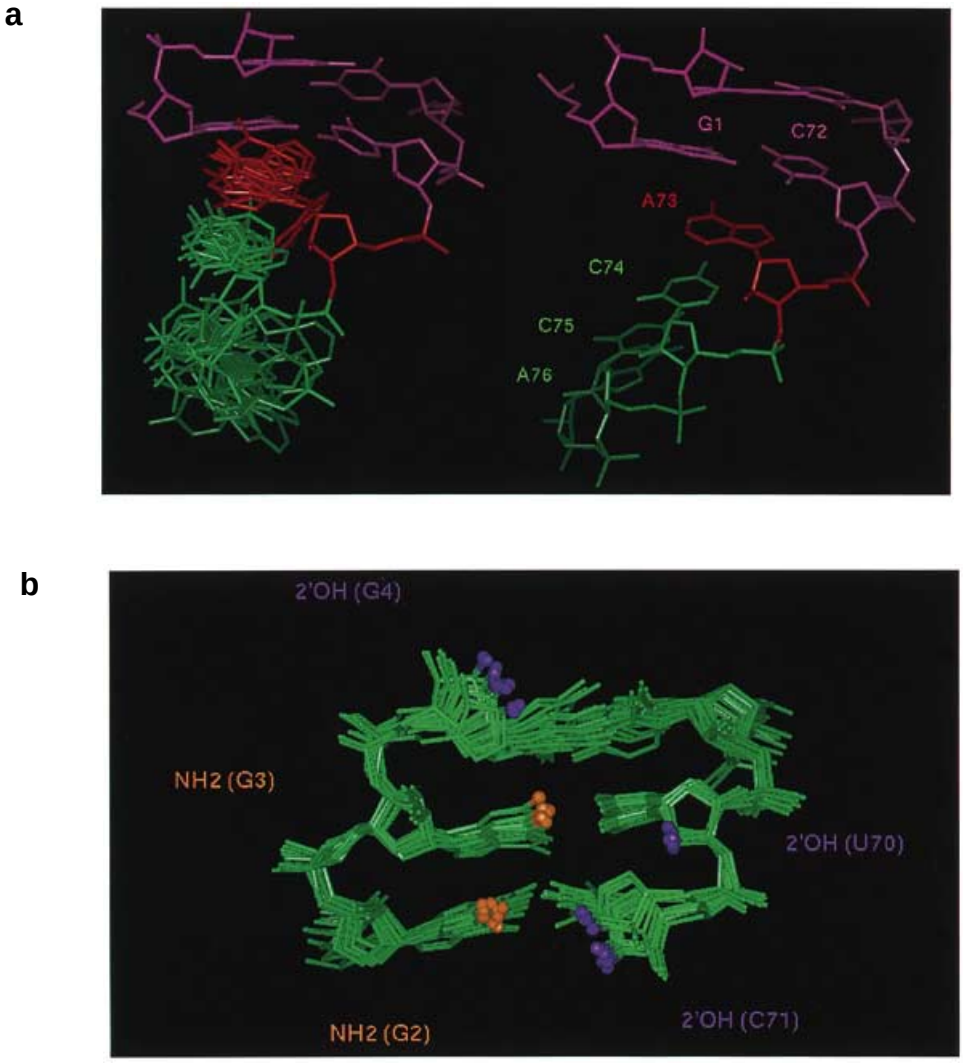

Figure 5. (**a**) Superimposition of 10 representative converged structures of the tRNA^{Ala} ACCA end (left) in comparison with a single strand of identical sequence derived from an A-form helix (right); notice the progressive loss of order towards the end of the single-stranded region. (**b**) View of the minor groove around the G3·U70 pair highlighting functional groups that are important for aminoacylation of tRNA^{Ala} acceptor end microhelices by AlaRS.

electrostatic potential to differentiate G·U sites from regular A-form helices. The location of the exocyclic amines of G2 and G3 and of phosphates and 2′-OH groups could define a set of functional groups in the minor groove for recognition of G3·U70 (Fig. 5b), as observed for the 3·70 pair in tRNA^{Ser} (2,10) and the G10·U25 pair in tRNA^{Asp} (6).

The importance of distortions from regular A-form helical geometry was revealed by the observation that G·A, C·A and U·U substitutions of the G3·U70 wobble pair preserve alanine identity *in vivo* (25,26). Partial alanine identity could also be conferred upon tRNA^{Lys} when the G3·C70 base pair was substituted by G·A or A·C (25). Functional groups in the minor and major grooves are not conserved at all between these mutants: unique structural features and/or helix deformability must therefore contribute substantially to tRNA^{Ala} identity. The present structure suggests three sites of potential importance for indirect recognition: the phosphodiester backbone surrounding G3, the 2′-hydroxyl and base functionalities of U70 and the distinctive G1·C72:A73 stacking interaction.

Recognition of the unusual structural features of the G·U pair and of the exocyclic amine of G3 may not only influence enzyme binding to RNA (K_m) but may also affect the efficiency of aminoacylation. The high K_m for tRNA–RS complexes (μM) limits the degree to which specificity can be achieved by binding alone. Consequently, discrimination of the G3·U70 base pair occurs both at the level of binding (K_m) and catalysis (k_{cat}) (49). The structural requirements for productive interaction at the G3·U70 site could affect catalysis by modulating amino acid binding (1) and/or catalytic efficiency. The reduced thermodynamic stability of the G·U-containing acceptor end may also facilitate optimization of the active site conformation by induced fit. The interaction between the discriminator base and the G1·C72 base pair may determine the orientation of the -CCA end in the transition state of catalysis, as suggested for tRNA^{Gln} (5,15) and tRNA^{fMet} (45,50). In this context, it is interesting to observe that tRNA^{Pro} is aminoacylated by AlaRS *in vitro* only when the 3·70 pair is mutated to G3·U70 and the end of the stem is converted to A73:G1·C72 (51), whereas the two separate mutants are essentially

Table 2. Average and r.m.s. deviations for selected helical parameters around the G·U wobble pair for the tRNA^{Ala} microhelix, the P1 helix structure (32), the tRNA^{Phe} acceptor stem (44) and the tRNA^{Asp} acceptor stem (40)

	tRNAAla	Incl.		DX (Å)		H-Twist	
GU-2/GU-1	G1•C72/G2•C71	12.4	±9.2	-2.4	±0.6	34.0	±2.8
GU-1/GU	G2•C71/G3•U70	12.8	±12.0	-2.8	±1.0	34.0	±3.0
GU/GU+1	G3•U70/G4•C69	25.2	±18.9	-4.9	±1.4	35.0	±7.3
GU+1/GU+2	G4•C69/C5•G68	6.7	±15.9	-2.4	±1.2	31.5	±2.6
	P1 helix	Incl.		DX(Å)		H-Twist	
GU-2/GU-1	A7•U14/A6•U15	3	±8	-1.9	±1.1	29	±2
GU-1/GU	A6•U15/U5•G16	-3	±16	-1.2	±1.1	39	±4
GU/GU+1	U5•G16/A4•U17	6	±10	-2.2	±0.8	32	±2
GU+1/GU+2	A4•U17/G3•C18	17	±9	-2.7	±1.0	37	±5
	tRNAPhe	Incl.		DX(Å)		H-Twist	
GU-2/GU-1	C2•G71/G3•C70	25.3		-4.5		32.0	
GU-1/GU	G3•C70/G4•U69	15.9		-3.8		32.6	
GU/GU+1	G4•U69A5•U68	14.2		-4.4		32.1	
GU+1/GU+2	A5•U68/U6•A67	13.0		-3.9		32.2	
	tRNAAsp	Incl.		DX(Å)		H-Twist	
GU-2/GU-1	A7•U66/G6•C67	33.9		-3.5		40.8	
GU-1/GU	G6•C67/U5•G68	12.5		-3.3		34.8	
GU/GU+1	U5•G68/G4•C69	2.3		-4.9		27.1	
GU+1/GU+2	G4•C69/C3•G70	21.0		-3.8		37.3	

inactive. A functional interaction with the A73:G1·C72 site could provide a mechanism to amplify and transfer to the active site any structural distortion induced by the G3·U70 base pair, thereby affecting the catalytic step.

ACKNOWLEDGEMENTS

We would like to thank Drs Fareed Aboul-ela and Frédéric H.-T.Allain and Mr Andreas Haaf for assistance with data acquisition and structure calculations and members of the NMR group here for suggestions and support.

REFERENCES

1 Ibba,M., Hong,K.-W., Sherman,J. M., Sever,A. and Söll,D. (1996) *Proc. Natl. Acad. Sci. USA*, **93**, 6953–6958.
2 Saks,M.E. and Sampson,J.R. (1996) *EMBO J.*, **15**, 2843–2849.
3 McClain,W.H. (1993) *FASEB J.*, **7**, 72–78.
4 McClain,W.H. (1995) In Söll,D. and RajBhandary,U. (eds), *tRNA: Structure, Biosynthesis and Function.* American Society for Microbiology, Washington, DC.
5 Rould,M.A., Perona,J.J., Söll,D. and Steitz,T.A. (1989) *Science*, **246**, 1135–1142.
6 Ruff,M., Krishnaswamy,S., Boeglin,M., Poterszman,A., Mitschler,A., Podjarny,A., Rees,B., Thierry,J.C. and Moras,D. (1991) *Science*, **252**, 1682–1689.
7 Biou,V., Yaremchuk,A., Tukalo,M. and Cusack,S. (1994) *Science*, **263**, 1404–1410.
8 Goldgur,Y., Mosyak,L., Reshetnikova,L., Ankilova,V., Lavrik,O., Khodyreva,S. and Safro,M. (1997) *Structure*, **5**, 59–68.
9 Cusack,S., Yaremchuk,A. and Tukalo,M. (1996) *EMBO J.*, **15**, 6321–6334.
10 Cusack,S., Yaremchuk,A. and Tukalo,M.(1996) *EMBO J.*, **15**, 2834–2842.
11 Rould,M.A. Perona,J.J. and Steitz,T.A. (1991) *Nature*, **352**, 213–218.
12 Caverelli,J., Rees,B., Ruff,M., Thierry,J.-C. and Moras, D. (1993) *Nature*, **362**, 181–184.
13 Hou,Y.-M. and P. Schimmel (1988) *Nature*, **333**, 140–145.
14 McClain,W.H. and Foss,K. (1988) *Science*, **240**, 793–796.
15 Gale,A.J., Shi,J.-P. and Schimmel,P. (1996) *Biochemistry*, **35**, 608–615.
16 Imura,N., Weiss,G.B. and Chambers,R.W. (1969) *Nature*, **222**, 1147–1148.
17 Francklyn,C. and Schimmel,P. (1989) *Nature*, **337**, 478–481.
18 Francklyn,C., Shi,J.-P. and Schimmel,P. (1992) *Science*, **255**, 1121–1125.
19 Musier-Forsyth,K., Shi,J.-P., Henderson,B., Bald,R., Fürste,J.P., Erdmann,V.A. and Schimmel,P. (1995) *J. Am. Chem. Soc.*, **117**, 7253–7254.
20 Doudna,J.A., Cormack,B.P. and Szostak,J.W. (1989) *Proc. Natl. Acad. Sci. USA*, **86**, 7402–7406.
21 Abramovitz,D.L., Friedman,R.A. Pyle,A.M. (1996) *Science*, **271**, 1410–1413.
22 Perrotta,A.T. and Been,M.D. (1996) *Nucleic Acids Res.*, **24**, 1314–1321.
23 Musier-Forsyth,K., Usman,N., Scaringe,S., Doudna,J.A., Green,R. and Schimmel,P. (1991) *Science*, **253**, 784–786.
24 Schimmel,P., Musier-Forsyth,K., Ibba,M. and Söll,D. (1996) *Nature*, **384**, 422.
25 McClain,W.H., Chen,Y.-M., Foss,K. and Schneider,J. (1988) *Science*, **242**, 1681–1684.
26 Gabriel,K., Schneider,J. and McClain,W.H. (1996) *Science*, **271**, 195–197.
27 Limmer,S., Reif,B., Ott,G., Arnold,L. and Sprinzl,M. (1996) *FEBS Lett.*, **385**, 15–20.
28 Limmer,S., Hofmann,H.-P., Ott,G. and Sprinzl,M. (1993) *Proc. Natl. Acad. Sci. USA*, **90**, 6199–6202.
29 Varani,G., Aboul-ela,F. and Allain,F.H.-T. (1996) *Prog. NMR Spectrosc.*, **29**, 51–127.
30 Batey,R.T., Battiste,J.L. and Williamson,J.R. (1995) *Methods Enzymol.*, **261**, 300–322.
31 Allain,F.H.-T. and Varani,G. (1995) *Nucleic Acids Res.*, **23**, 341–350.
32 Allain,F.H.-T. and Varani,G. (1995) *J. Mol. Biol.*, **250**, 333–353.
33 Aboul-ela,F., Karn,J. and Varani,G. (1995) *J. Mol. Biol.*, **253**, 313–332.
34 Varani,G., Aboul-ela,F., Allain,F.H.-T. and C. C. Gubser (1995) *J. Biomol. NMR*, **5**, 315–320.
35 Brünger,A.T. (1990) *X-PLOR Manual.* Yale University Press, New Haven, CT.
36 Avis,J., Allain,F.H.-T., Howe,P.W.A., Varani,G., Neuhaus,D. and Nagai,K. (1996) *J. Mol. Biol.*, **257**, 398–411.
37 Diamond,R. (1995) *Acta Crystallogr.*, **D51**, 127–135.
38 Babcock,M.S., Pednault,E.P.D. and Olson,W.K. (1993) *J. Biomol. Struct. Dyn.*, **11**, 597–628.
39 Allain,F.H.-T. and Varani,G. (1997) *J. Mol. Biol.*, **267**, 338–351.
40 Moras,D., Dumas,P. and Westhof,E. (1986) van Knippenberg,P.H. and Hilbers,C.W. (eds), In *Structure and Dynamics of RNA.* Plenum Press, New York, NY.
41 Wang,Y.-X., Huang,S. and Draper,D.E. (1996) *Nucleic Acids Res.*, **24**, 2666–2672.
42 Lietzke,S.E., Barnes,C.L., Berglund,J.A. and Kundrot,C.E. (1996) *Structure*, **4**, 917–930.
43 Wu,M. and Turner,D.H. (1996) *Biochemistry*, **35**, 9677–9689.
44 Ladner,J.E., Jack,A., Robertus,J.D., Brown,R.S., Rhodes,D., Clark,B.F.C. and Klug,A. (1975) *Proc. Natl. Acad. Sci. USA*, **72**, 4414–4418.
45 Viani Puglisi,E., Puglisi,J.D., Williamson,J.R. and RajBhandary,U.L. (1994) *Proc. Natl. Acad. Sci. USA*, **91**, 11467–11471.
46 Musier-Forsyth,K. and Schimmel,P. (1992) *Nature*, **357**, 513–515.
47 Ott,G., Arnold,L. and Limmer,S. (1993) *Nucleic Acids Res.*, **21**, 5859–5864.
48 Cate,J.H. and Doudna,J.A. (1996) *Structure*, **4**, 1221–1229.
49 Park,S.J., Hou,Y.-M. and Schimmel,P. (1989) *Biochemistry*, **28**, 2740–2746.
50 Lee,C.P., Mandal,N., Dyson,M.R. and RajBhandary,U.L. (1993) *Proc. Natl. Acad. Sci. USA*, **90**, 7149–7152.
51 Liu,H., Yap,L.-P. and Musier-Forsyth,K. (1996) *J. Am. Chem. Soc.*, **118**, 2523–2524.